Available online at www.sciencedirect.com
SCIENCE DIRECT®

Journal of the European Ceramic Society 23 (2003) 2023–2029
www.elsevier.com/locate/jeurceramsoc

Oxidation behavior of liquid-phase sintered SiC with AlN and Er_2O_3 additives between 1200 °C and 1400 °C

Shuqi Guo*, Naoto Hirosaki, Hidehiko Tanaka, Yoshinobu Yamamoto, Toshiyuki Nishimura

Advanced Materials Laboratory, National Institute for Materials Science, 1-1 Namiki, Tsukuba, Ibaraki 305-0044, Japan

Received 2 September 2002; accepted 13 January 2003

Abstract

The oxidation behavior of liquid-phase sintered SiC, with AlN and Er_2O_3 additives, was investigated in air between 1200 °C and 1400 °C, for up to 200 h. The material showed high oxidation resistance at and below 1300 °C, however, the oxidation resistance degraded significantly at 1400 °C. The parabolic weight gain versus oxidation time was measured only for the period of 30–200 h. The apparent oxidation activation energy, Q, was determined to be ≈600 kJ/mol. The major oxidation products consisted of SiO_2 (α-cristobalite) and $Er_2Si_2O_7$. These oxidation products crystallized from the surface amorphous silicate phase during oxidation. The morphology of the microstructure of the oxidized surfaces was shown to be dependent on oxidation temperature. The most probably rate-limiting step was the migration of additive cations along the residual intergranular amorphous phase to the interface between the oxide layer and the SiC bulk.

Keywords: AlN; Er_2O_3; Liquid phase sintering; Oxidation; SiC

1. Introduction

Silicon carbide (SiC) ceramics have become an important class of materials for structural applications at elevated temperatures. However, it is difficult to densify pure silicon carbide ceramics without sintering additives because SiC is a highly covalent material bonded compound. To achieve densification of pure SiC ceramics, a sintering addition is necessary during the sintering process. Boron and carbon additions drastically improved the shrinkage kinetics of SiC and densified SiC ceramics during the solid-state sintering process.[1,2] When oxides are added to pure silicon carbide, on the other hand, formation of an intergranular liquid phase aids the densification of silicon carbide during the sintering process.[3–5] One of advantages for the liquid-phase sintered SiC is its high fracture toughness (~8 MPa $m^{1/2}$),[6] compared to that for the solid-state sintered SiC (~3 MPa $m^{1/2}$),[2] because of the formation of elongated grains during the liquid-phase sintering process. However, it is a common feature that an intergranular amorphous phase is present between SiC grains for liquid-phase sintered SiC ceramics, resulting from SiC particles reaction with the liquid additive during the sintering process.[4,5] Although the amorphous phase is not a substantial phase in terms of the volume that it occupies, this phase has a significant effect on the high-temperature mechanical properties.[7,8] There are two effective methods for improving the high-temperature properties of silicon carbide materials to increase the refractoriness of the grain boundary phase and to promote crystallization of the amorphous phase. This may be achieved by the selection appropriate additives and chemical compositions.

Liquid-phase sintered silicon carbide, with AlN and Y_2O_3 additives, has been reported early by Chia et al.[9] and by Nader.[10] Recently, Kim et al.[11,12] have developed a new type of liquid-phase sintered silicon carbide, with AlN and Re_2O_3 (Re = Yb and Er). A significant improvement in the high-temperature strength for the

* Corresponding author at: Kagawa Laboratory, Institute of Industrial Science, The University of Tokyo, 4-6-1 Komaba, Meguro-ku, Tokyo 153-8505, Japan. Tel.: +81-3-5452-6328; fax: +81-3-5452-6329.
E-mail address: guo@iis.u-tokyo.ac.jp (S. Guo).

0955-2219/03/$ - see front matter © 2003 Elsevier Science Ltd. All rights reserved.
doi:10.1016/S0955-2219(03)00030-X

silicon carbide material has been reported.[11,12] However, the oxidation behavior of this material is little known. Although oxidation behavior of solid-state sintered SiC materials has been extensively studied,[13–16] this behavior of liquid-phase sintered SiC material with Re_2O_3 additives is expected to be different because the residual intergranular amorphous phase is present between SiC grains for this material. Furthermore, the application of ceramics to energy conversion system depends on the mechanical reliability of the ceramic during thermal exposure to oxidizing conditions at high temperatures. Therefore, it is required for this material to learn oxidation behavior at elevated temperature. The aim of this work was to study in detail the oxidation behavior of liquid-phase sintered SiC material, with AlN and Er_2O_3 additives, in the temperature range of 1200–1400 °C.

2. Experimental procedure

2.1. Material

The SiC ceramic used in the present study was liquid-phase sintered from a ball-milled mixture of SiC, and AlN and Er_2O_3 additives, with the composition 79.6 wt.% β-SiC, 0.8 wt.% α-SiC, 2.7 wt.% AlN and 16.9 wt.% Er_2O_3. The starting powders were α-SiC (A-1 grade, Showa Denko, Tokyo, Japan), β-SiC (Ultrafine grade, Betarundum, Ibiden Co., Ltd., Ogaki, Japan), AlN (Grade F, Tokuyama Soda Co., Tokyo, Japan), and Er_2O_3 (99.9% purity, Shinetsu Chemical Co., Ltd., Tokyo, Japan). The mean particle sizes of the α-SiC and the β-SiC powders were 0.45 and 0.27 μm in diameter respectively. The specific surface areas of both powders were 15 and 17.5 m^2/g respectively. A mixture of Er_2O_3 and AlN was added to SiC, and then the powder batches were mixed in ethanol for 2 h, using a SiC milling media, and subsequently dried in a rotation evaporator. The dried powder was die-pressed into rectangular shaped samples, 80 mm×45 mm×13 mm, at room temperature under 20 MPa. The samples were placed in a BN-coated graphite die and sintered for 7 h at 1900 °C under a pressure of 20 MPa, in a dry N_2 atmosphere, using a gas pressure sintering furnace (FVPHR-R-10, FRET-40, Fuji Electric Co., Ltd., Tokyo, Japan).

The liquid-phase sintered SiC ceramic with AlN and Er_2O_3 additives densified to a high relative density of >97%. X-ray diffraction of the as-received SiC material exhibited the presence of a major crystalline α-SiC phase and a minor crystalline β-SiC phase, together with a major $Er_4Si_2O_7N_2$ secondary phases. Transmission electron microscopy confirmed a thin (9 Å) residual amorphous film at two-grain boundaries.[11]

2.2. Oxidation test

Specimens, averaging 40 mm×4 mm×3 mm in size, were cut from the sintered plates, using a conventional mechanical cutting procedure. The surfaces of the specimens were ground with an 800-grit diamond wheel and then the surface was polished with diamond paste up to 0.5 μm. Finally, the edges of the specimen were chamfered at 45°. The polished specimens were ultrasonically cleaned in acetone and then kept in an oven, at a constant temperature of 100 °C, prior to oxidation. Oxidation tests were performed at 1200 °C, 1300 °C and 1400 °C over a period of 200 h in air. The specimens were supported on pure Al_2O_3 knife-edged fixtures in an electronic furnace (SSFT-1520, Nikkato Co., Ltd., Tokyo, Japan). The heating and cooling rates were 20 °C and 10 °C/min respectively. Dry air is passed through the electron furnace at ~300 cm^3/min during heating. Before and after oxidation, the specimens were weighed using an analytical balance (MT5, Mettler Toledo Co., Ltd., Switzerland) with an accuracy of ±0.001 mg. After oxidation, the specimens were examined using X-ray diffraction (XRD) to determine the oxidation products produced. The oxidized surfaces were characterized by scanning electron microscopy (SEM) and energy-dispersive X-ray spectroscopy (EDX).

3. Results

3.1. Oxidation kinetics

The weight gain data from oxidation of the liquid-phase sintered SiC between 1200 °C and 1400 °C are summarized in Fig. 1. After 200 h oxidation at 1200 °C and 1300 °C, this material has specific weight gains of 0.247 and 0.704 mg/cm^2 respectively, showing high oxidation resistance. The high oxidation resistance was attributable to the raised refractoriness of the intergranular

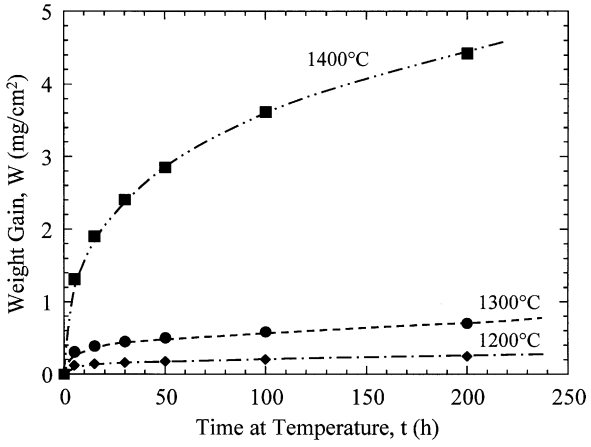

Fig. 1. Plots of specific weight gain as a function of time between 1200 °C and 1400 °C.

amorphous phase.[11] When the oxidation temperature was raised up to 1400 °C, however, the specific weight gain increased sharply and was determined to be 4.426 mg/cm^2 after 200 h oxidation. This indicated that the oxidation resistance of the material degraded significantly at 1400 °C. The oxidation of liquid-phase sintered silicon carbide has been shown to be the parabolic behavior, which can be represented by the following relation[17]

$$W^2 = kt \tag{1}$$

where W is the weight gain per unit surface area, t is the exposure time at a given temperature, k is the parabolic oxidation rate constant and is dependent on the temperature, T. Plotting these data parabolically, the oxidation of the studied material is not found to display parabolic kinetics until after about 30 h oxidation for all temperature, as shown in Fig. 2. In particular, the oxidized samples at 1300 °C and 1400 °C appear to be the significantly deviating from parabolic behavior. After 30 h oxidation, the parabolic behavior is observed for each curve. However, additional data corresponding to longer oxidation time may be needed to distinguish whether the oxidation behavior of the studied material is parabolic or not. To calculate parabolic rate constant, k, of the studied material, it is assumed that this material follows the parabolic behavior for the period of 30–200 h.

The parabolic rate constant, k, follows the Arrhenius law

$$k = k_0 \exp\left(-\frac{Q}{RT}\right) \tag{2}$$

where k_0 is a frequency factor, Q is the oxidation activation energy (both k_0 and Q are material constants), T is the absolute temperature and R is the gas constant. The k values at different temperatures can be determined from the slopes of the straight lines in Fig. 2. Note that the parabolic rate constant was determined for the period of 30–200 h in which the parabolic oxidation behavior was shown (Fig. 2). Plots of the k values obtained as a function of temperature are shown in Fig. 3. The apparent oxidation activation energy was determined from the data shown in Fig. 3. The Q was found to be 600 kJ/mol for the liquid-phase sintered SiC material oxidized in air between 1200 °C and 1400 °C.

3.2. Phase composition of oxidized surfaces

The phases identified by X-ray diffraction in the unoxidized and oxidized surfaces of the liquid-phase sintered SiC ceramic are summarized in Table 1. The XRD patterns of the oxidized surface identified that crystalline β-$Er_2Si_2O_7$ and SiO_2 (α-cristobalite) phases are the major oxidation products for each oxidation temperature. α-SiC, β-SiC and trace amounts of $Er_4Si_2O_7N_2$ and Er_2SiO_5 were present for each oxidized specimen. The intensity of the α-SiC, β-SiC and $Er_4Si_2O_7N_2$ peaks decreased with increasing oxidation temperature, indicating these signals were from the bulk

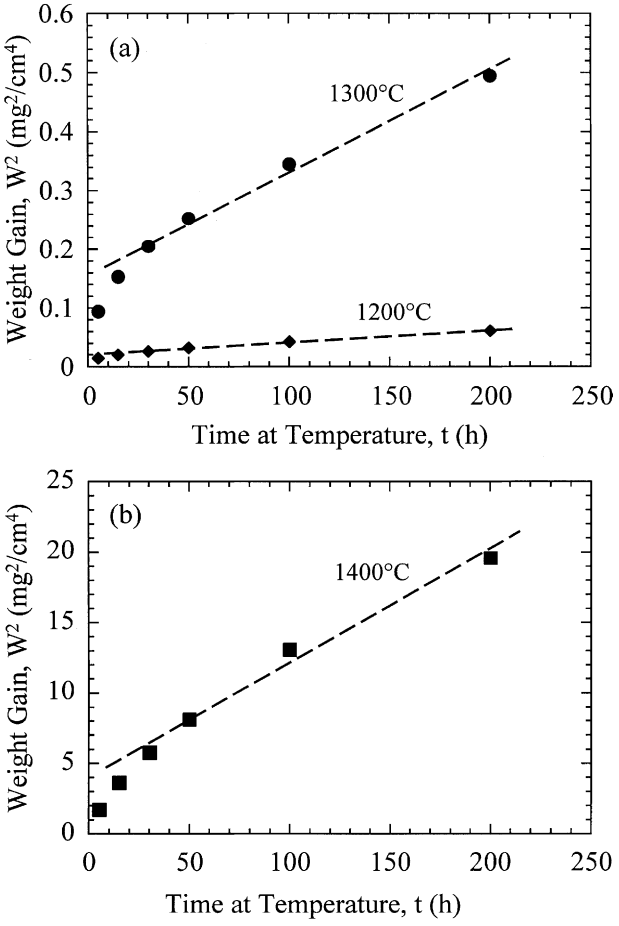

Fig. 2. Square of weight gain as a function of time, at (a) 1200 °C and 1300 °C, and (b) 1400 °C.

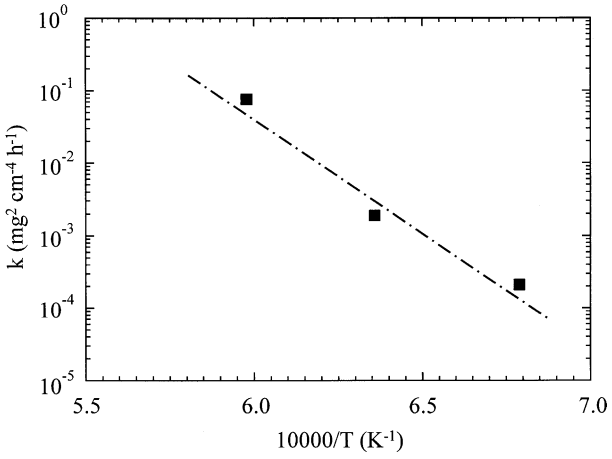

Fig. 3. Plots of oxidation rate constants as a function of oxidation temperature.

Table 1
X-ray diffraction of the unoxidized and the oxidized surfaces

	Oxidized		
	1200 °C	1300 °C	1400 °C
α-SiC	α-SiC	α-SiC	α-SiC
β-SiC	β-SiC	β-SiC	β-SiC
$Er_4Si_2O_7N_2$	Er_2SiO_5	Er_2SiO_5	Er_2SiO_5
	$Er_4Si_2O_7N_2$	$Er_4Si_2O_7N_2$	$Er_4Si_2O_7N_2$
	$Er_2Si_2O_7$	$Er_2Si_2O_7$	$Er_2Si_2O_7$
	SiO_2[a]	SiO_2[a]	SiO_2[a]

[a] As α-cristobalite.

ceramic beneath the oxidized surface layer. In addition, new peaks of Er_2SiO_5 were detected for each oxidized specimen.

3.3. Morphology of oxidized surfaces

The morphologies of the surfaces oxidized between 1200 °C and 1400 °C for 200 h are shown in Fig. 4. In each micrograph the phase in the brightest contrast is the rare-earth disilicates ($Er_2Si_2O_7$) and the background consists of SiO_2 (α-cristobalite) and the residual amorphous silicate phase. $Er_2Si_2O_7$ and the cristobalite grains crystallized from the amorphous silicate phase on the oxidized surface. Two distinct morphologies, an equiaxed and plate-like type, were revealed for the rare-earth disilicates, dependent on oxidation temperature. At 1200 °C, the oxidized surface consisted of the equiaxed $Er_2Si_2O_7$ crystals. At 1300 °C, the surface consisted of $Er_2Si_2O_7$ in a plate-like morphology, but the equiaxed form still predominated. At 1400 °C, however, the surface contained $Er_2Si_2O_7$ of the plate-like morphology. Furthermore, the grains of $Er_2Si_2O_7$ coarsen rapidly and the content increased rapidly with increasing oxidation temperature; at 1300 °C the oxidized surface was almost completely covered with the larger $Er_2Si_2O_7$ grains [Fig. 4(b)] and at 1400 °C the surface was covered with the bigger plate-like $Er_2Si_2O_7$ grains [Fig. 4(c)]. Moreover, either spalling of the oxide layer from the substrate or the cracking of the oxide layer was not observed in any instance (Fig. 4).

Table 2
EDX analysis results of the composition of the oxidized surfaces

		Composition (at.%)					
		C	Si	N	O	Er	Al
1200 °C, 200 h	Bright	8.47	18.16	2.00	53.70	17.68	0.00
	Black	4.43	32.66	3.39	58.63	0.28	0.63
1300 °C, 200 h	Bright	9.68	17.88	2.44	52.06	16.78	1.17
	Black	6.24	28.66	2.38	51.78	2.17	8.76
1400 °C, 200 h	Bright	6.96	16.06	2.43	57.50	17.05	0.00
	Black	3.08	20.93	2.04	55.70	4.92	13.33

The compositions of the bright region and background in the oxidized surfaces between 1200 °C and 1400 °C for 200 h were analyzed by EDX, the results of which are summarized in Table 2. The concentrations of Al and Er in the surface silicate phase increase with increasing oxidation temperature, conversely, the concentration of N and Si decreases. The concentration of C in the surface silicate phase is higher for the sample oxidized at 1200 °C than for the sample oxidized at 1300 °C, for the sample oxidized at 1400 °C, however,

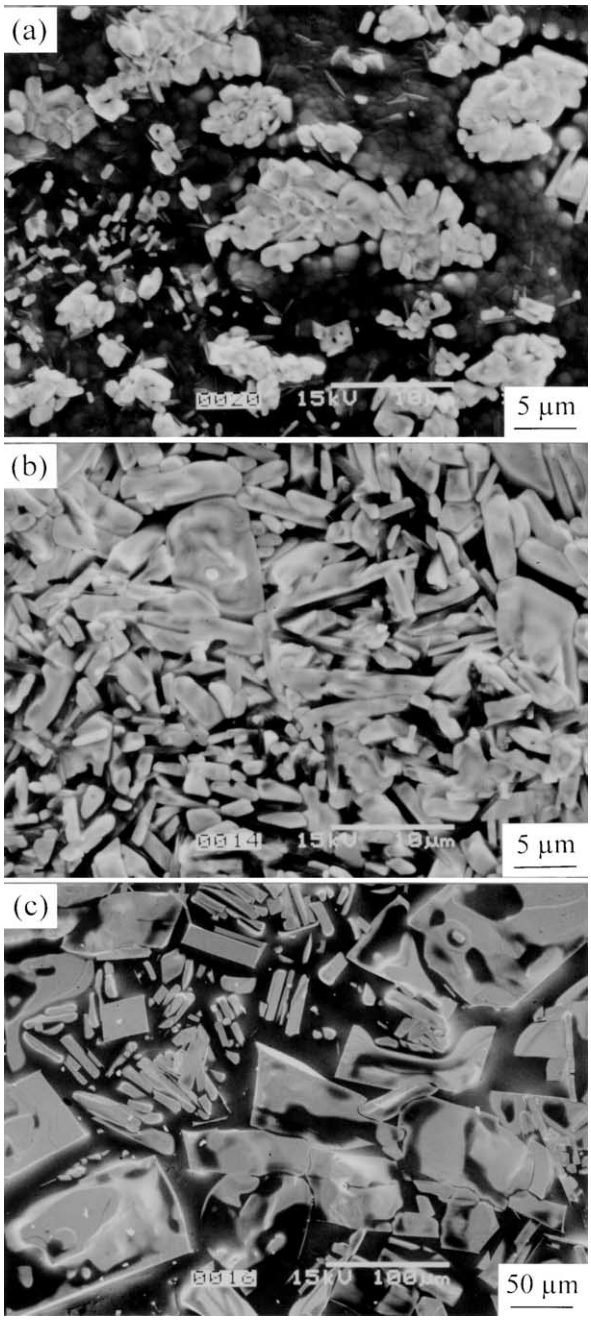

Fig. 4. SEM micrographs of the oxidized surfaces after 200 h oxidation, at (a) 1200 °C, (b) 1300 °C, and (c) 1400 °C, showing surface topography and morphology.

the content of C is the lowest among all oxidized samples. On the other hand, the concentrations of Er, Si and O represented by bright regions in Fig. 4 ($Er_2Si_2O_7$ phase) were slightly dependent on oxidation temperature, and the ratio of Er:Si:O is approaching to 2:2:7. C and N were detected in the disilicate for overall oxidation temperature, whereas the trace amount of Al was present only for the sample oxidized at 1300 °C.

Fig. 5 shows the typical SEM micrographs of the transverse cross-section of the samples oxidized between 1200 °C and 1400 °C. A dense oxidized layer was observed on the surfaces of all oxidized samples. The oxide layer thickness was determined to be approximately 1 μm at 1200 °C, 4 μm at 1300 °C and 40 μm at 1400 °C. A few of pores were observed at and/or near the interface between the oxidized layer and SiC bulk for the samples oxidized at 1200 °C and 1300 °C [indicated by arrows in Fig. 5(a) and (b)]. In the contrast, many pores were seen in a region of the oxide layer near the SiC bulk for the sample exposed at 1400 °C [Fig. 5(c)].

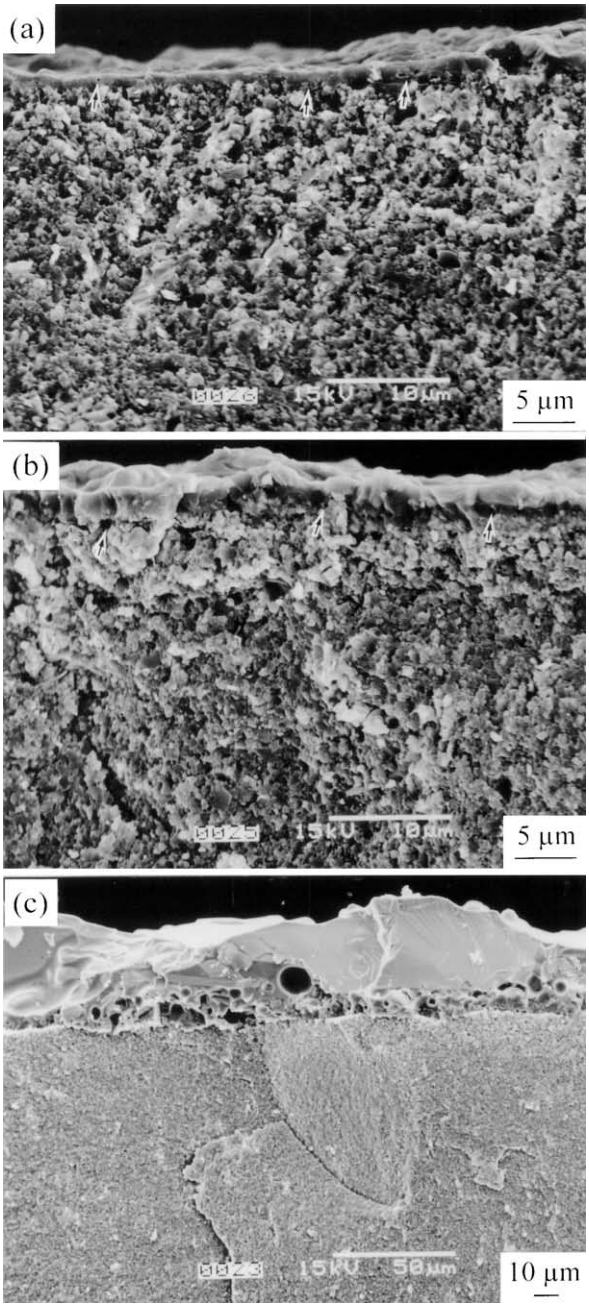

Fig. 5. Typical SEM micrographs of the transverse cross-sections of the oxidized specimens, at (a) 1200 °C, (b) 1300 °C, and (c) 1400 °C for 200 h.

4. Discussion

4.1. Oxidation mechanism

The parabolic oxidation kinetics exhibited by solid-state sintered silicon carbide ceramics were originally assumed to be the result of a diffusion of oxidant through the oxide to the growth interface.[13–15] However, high-temperature oxidation of liquid-phase sintered silicon carbide with oxide additives leads to accelerated oxidation (Figs. 1 and 2). This is attributable to the enhanced oxidation of SiC dissolved in a highly viscous silicate phase present at the oxidized surface. EDX composition analysis revealed that the compositional concentrations in the oxidized surface have been changed with increasing oxidation temperature (Table 2). This suggests that the outward diffusion of both the additive cations and nitrogen and the inward diffusion of oxygen occurred during oxidation, as a result of the presence of the rich-impurities residual amorphous phase at the grain boundaries.[11] This diffusion behavior results in a compositional gradient beneath oxide layer. Thus, the oxidation kinetics observed in this work was attributed to the outward diffusion of additive cations (Er^{3+} and Al^{3+}) and nitrogen, produced from the amorphous intergranular-phase/oxide-layer diffusion couple, and to the inward diffusion of oxygen. However, the oxidation of the studied material is not found to display parabolic oxidation kinetics until after about 30 h oxidation for all temperature (Fig. 2). The material shows faster oxidation rate up to about 30 h, and then the rate slows down with increasing time. This may be caused by the rapid increasing of the thickness of erbium- and aluminum-depletion zone beneath the oxidized layer with increasing oxidation time, which requires longer time for diffusion of additive cations, resulting in the decrease in oxidation rate with increasing time.

In previous study,[15] it was shown that the SiC phase oxidized to form SiO_2 according to the following three possible equations;

$$SiC(s) + O_2(g) = SiO_2(s) + C(s) \quad (3a)$$

$$SiC(s) + 1.5O_2(g) = SiO_2(s) + CO(g) \quad (3b)$$

$$SiC(s) + 2O_2(g) = SiO_2(s) + CO_2(g) \quad (3c)$$

EDX compositional measurement in the oxidized surfaces showed that the concentration of C is the highest for the sample oxidized at 1300 °C and it is the lowest for the sample oxidized at 1400 °C (Table 2). Furthermore, SEM observations of the transverse cross-section exhibited for the samples oxidized at 1200 °C and 1300 °C only a few of small pores was present at and/or near interface between the oxide layer and the SiC bulk [Fig. 5(a) and (b)]. For the sample oxidized at 1400 °C, however, a number of the larger pores were observed [Fig. 5(c)]. The presence of the pores indicated that gas was trapped in the oxide layer due to gas bubbles, which nucleate near the oxidation front.[18,19] Based on these experimental measurements and observations, it is presumed that equation (3a) was a predominant reaction during oxidation when the samples were exposed to 1200 °C and 1300 °C and Eqs. (3b) and (3c) became more important for the sample exposed to 1400 °C.

In addition, because $Er_4Si_2O_7N_2$ phase is instable as it was exposed to oxidation environment at high temperature, i.e., $Er_4Si_2O_7N_2$ phase cannot coexist with SiO_2 (product of oxidation), thus its decomposition occurred simultaneously, accompanying SiC oxidation, according to the following equation[19,20]

$$2Er_4Si_2O_7N_2(s) + 3O_2(g) = 4Er_2SiO_5(s) + 2N_2(g) \quad (4)$$

Subsequently, Er_2SiO_5 phase, which is the oxidation product of $Er_4Si_2O_7N_2$, reacts with SiO_2 to form $Er_2Si_2O_7$ as follows;[19,20]

$$Er_2SiO_5(s) + SiO_2(s) = Er_2Si_2O_7(s) \quad (5)$$

Eqs. (4) and (5) are similar to those observed in oxidized Si_3N_4 ceramics with oxide additives.[19,20] In this study, after oxidation, new peaks of Er_2SiO_5 phase were detected and some peaks of $Yb_4Si_2O_7N_2$ phase disappeared. This suggests that reactions (4) and (5) occurred during oxidation.

The experimental value of the apparent activation energy for oxidation (600 kJ/mol) is higher than the activation energy obtained in solid-state sintered SiC ceramics (84–498 kJ/mol).[13–15] This discrepancy is probably associated with the composition of the residual intergranular amorphous phase present at grain-boundaries. Babini et al.[21] reported the apparent activation energy for oxidation of 260–623 kJ/mol, depending on the composition, for Y_2O_3–SiO_2-doped hot-pressed Si_3N_4 ceramic oxidized in air between 1000 °C and 1400 °C. Similar composition dependence of apparent activation energy, although not well known, is expected for the liquid-phase sintered SiC material investigated in this study. This suggests that diffusion of additive cations through the residual intergranular amorphous phase to the interface between the SiC bulk and the oxide layer as the most probable rate-limiting step for oxidation of the studied material.

4.2. Morphology of oxidized surfaces

SEM observations of the oxidized surfaces revealed that present was $Er_2Si_2O_7$ phase either in the equiaxed or in plate-like morphologies, dependent on oxidation temperature (Fig. 4). Babini et al.[22] have reported the oxidation temperature dependence of the morphology of the crystalline disilicate phase in the oxidized surface of $Y_2Si_2O_7$–Si_3N_4 material. They concluded that the amount and morphology of crystalline disilicate phases in the oxidized surface were determined by solubility and mobility of additive and impurity cations, which were closely related to oxidation temperature. Studies[19,23] have been reported recently that the formation of the disilicates of the equiaxed morphology in Si_3N_4 materials with Re_2O_3 (Re = Y, Yb, Er and Sm) during oxidation is associated with the very low concentration of impurities in oxidized surface. In the present study, the concentration of Al increases rapidly with increasing oxidation temperature, and its content is about 20 times more in the oxidized surface at 1400 °C than in the surface at 1200 °C (Table 2). It is likely that Al acts to catalyze the growth of the $Er_2Si_2O_7$ crystals along preferred planes to form high aspect ratios resulting from highly anisotropic growth rates [Fig. 4(c)].

5. Conclusions

The oxidation behavior of liquid-phase sintered SiC ceramic, with AlN and Er_2O_3 additives, was investigated in air between 1200 °C and 1400 °C, for up to 200 h. The major results obtained are exhibited below:

1. The liquid-phase sintered SiC ceramic with AlN and Er_2O_3 additives exhibited high oxidation resistance at and/or below 1300 °C. This was attributable to the raised refractoriness of the residual intergranular amorphous phase. However, the oxidation resistance degraded significantly at 1400 °C.
2. The oxidation of the studied material was not found to display parabolic behavior until after about 30 h oxidation for all oxidation temperatures. The parabolic weight gain versus oxidation time was measured only for the period of 30–200 h.
3. The apparent oxidation activation energy was found to be 600 kJ/mol. The most probably rate-limiting step was the migration of additive cations along the residual intergranular amorphous phase to the interface between the oxide layer and the SiC bulk.

4. The major oxidation products consisted of SiO_2 (α-cristobslite) and $Er_2Si_2O_7$. The $Er_2Si_2O_7$ and SiO_2 grains crystallized from the surface silicate phase during the oxidation. The morphology of the microstructure of the oxidized surfaces depended on oxidation temperature.

References

1. Prochazka, S., The role of boron and carbon in the sintering of silicon carbide. In *Special Ceramics 6*, ed. P. Popper. Br. Ceramic Research Association, Stoke-on-Trent, UK, 1975, pp. 171–181.
2. Faber, K. T. and Evans, A. G., Intergranular crack-deflection toughening in silicon carbide. *J. Am. Ceram. Soc.*, 1983, **66**(6), C94–C96.
3. Cutler, R. A. and Jackson, T. B., Liquid-phase sintered silicon carbide. In *Ceramic Materials and Components for Engines, Proceeding of the Third International Symposium*, ed. V. J. Tennery. American Ceramics Society, Westerville, OH, 1989, pp. 309–318.
4. Padture, N. P. and Lawn, B. R., Toughness properties of a silicon carbide with an in situ induced heterogeneous grain structure. *J. Am. Ceram. Soc.*,, 1994, **77**(10), 2518–2522.
5. Mitomo, M., Kim, Y.-W. and Hirotsuru, H., Fabrication of silicon carbide nanoceramics. *J. Mater. Res.*, 1996, **11**(7), 1601–1604.
6. Padture, P., In situ-toughened silicon carbide. *J. Am. Ceram. Soc.*, 1994, **77**(2), 519–523.
7. Keppeler, M., Reicher, H.-G., Broadley, J. M., Thum, G., Wiedmann, I. and Aldinger, F., High temperature mechanical behavior of liquid-phase sintered silicon carbide. *J. Eur. Ceram. Soc.*, 1998, **19**, 521–526.
8. Jou, Z. C., Virkar, A. V. and Culter, R. A., High temperature creep of SiC densified using a transient liquid phase. *J. Mater. Res.*, 1991, **6**(9), 1945–1949.
9. Chia, K. Y., Boecker, W. D. G., Storm, R. S., US Patent 5298470, 1994.
10. Nader, M. Untersuchung der Kornwachstumsphänomene an Flüssigphasengesinterten SiC-Keramiken und ihre Möglichkeit zur Gefügeveränderung. PhD thesis, University of Stuttgart, Stuttgart, 1995 (in German).
11. Kim, Y.-W., Mitomo, M. and Nishimura, T., Heat-resistant silicon carbide with aluminum nitride and erbium oxide. *J. Am. Ceram. Soc.*, 2001, **84**(9), 2060–2064.
12. Kim, Y.-W., Mitomo, M. and Nishimura, T., High-temperature strength of liquid-phase-sintered SiC with AlN and Re_2O_3 (RE = Y, Yb). *J. Am. Ceram. Soc.*, 2002, **85**(4), 1007–1009.
13. Singhal, S. C., Oxidation kinetics of hot-pressed SiC. *J. Mater. Sci.*, 1976, **11**, 1246–1253.
14. Costello, J. A. and Tressler, R. E., Oxidation kinetics of hot-pressed SiC and sintered α-SiC. *J. Am. Ceram. Soc.*, 1981, **64**(5-6), 327–331.
15. Costello, J. A. and Tressler, R. E., Oxidation kinetics of silicon carbide crystals and ceramics: I, in dry oxygen. *J. Am. Ceram. Soc.*, 1986, **69**(9), 674–681.
16. Berton, B., Bacos, M. P., Demange, D. and Lahaye, J., High-temperature oxidation of silicon carbide in simulated atmospheric re-entry condition. *J. Mater. Sci.*, 1992, **27**, 3206–3210.
17. Choi, H. J., Lee, J. G. and Kim, Y. W., Oxidation behavior of liquid-phase sintered silicon carbide with aluminum nitride and rare-earth oxides. *J. Am. Ceram. Soc.*, 2002, **85**(9), 2281–2286.
18. Guo, S. Q., Hirosaki, N., Yamamoto, Y., Nishimura, T. and Mitomo, M., Strength retention in hot-pressed Si_3N_4 ceramics with Lu_2O_3 additives after oxidation exposure in air at 1500 °C. *J. Am. Ceram. Soc.*, 2002, **85**(6), 1607–1609.
19. Guo, S. Q., Hirosaki, N., Nishimura, T., Yamamoto, Y. and Mitomo, M., Oxidation behavior and strength degradation of a Yb_2O_3–SiO_2-doped hot-pressed silicon nitride between 1200 °C and 1500 °C. *Phil. Mag. A*, 2002, **82**(16), 3027–3043.
20. Choi, H. J., Lee, J. G. and Kim, Y. W., Oxidation behavior of hot-pressed Si_3N_4 with Re_2O_3 (Re = Y, Yb, Er, La). *J. Eur. Ceram. Soc.*, 1999, **19**, 2757–2762.
21. Babini, G. N., Bellosi, A. and Vincenzini, P., A diffusion model for the oxidation of hot-pressed Si_3N_4–Y_2O_3–SiO_2 materials. *J. Mater. Sci.*, 1984, **19**, 1029–1042.
22. Babini, G. N., Bellosi, A. and Vincenzini, P., Factors influencing structural evolution in the oxide of hot-pressed Si_3N_4–Y_2O_3–SiO_2 materials. *J. Mater. Sci.*, 1984, **19**, 3487–3497.
23. Cinibulk, M. K., Thomas, G. and Johnson, S. M., Oxidation behavior of rare-earth disilicate-silicon nitride ceramics. *J. Am. Ceram. Soc.*, 1992, **75**(8), 2044–2049.